Solving Inverse Problems in Protein Space Using Diffusion-Based Priors

Axel Levy®*
Stanford University

Eric R. Chan

Stanford University

Sara Fridovich-Keil[®] Stanford University

Frédéric Poitevin®
SLAC National Accelerator Laboratory

Ellen D. Zhong[®]
Princeton University

Gordon Wetzstein^{®*}
Stanford University

axel-levy.github.io/adp-3d

Abstract

The interaction of a protein with its environment can be understood and controlled via its 3D structure. Experimental methods for protein structure determination, such as X-ray crystallography or cryogenic electron microscopy, shed light on biological processes but introduce challenging inverse problems. Learning-based approaches have emerged as accurate and efficient methods to solve these inverse problems for 3D structure determination, but are specialized for a predefined type of measurement. Here, we introduce a versatile framework to turn raw biophysical measurements of varying types into 3D atomic models. Our method combines a physics-based forward model of the measurement process with a pretrained generative model providing a task-agnostic, data-driven prior. Our method outperforms posterior sampling baselines on both linear and non-linear inverse problems. In particular, it is the first diffusion-based method for refining atomic models from cryo-EM density maps.

1 Introduction

Our ability to understand the molecular machinery of living organisms and design therapeutic compounds depends on our capability to observe the three-dimensional structures of protein and other biomolecular complexes. Experimental methods in structural biology such as X-ray crystallography, cryogenic electron microscopy (cryo-EM) and nuclear magnetic resonance (NMR) spectroscopy provide noisy and partial measurements from which the 3D structure of these biomolecules can be inferred. However, turning experimental observations into reliable 3D structural models is a challenging computational task. For many years, reconstruction algorithms were based on Maximum-A-Posteriori (MAP) estimation and often resorted to hand-crafted priors to compensate for the ill-posedness of the problem. State-of-the-art algorithms for cryo-EM reconstruction [56, 52] are instances of such "white-box" algorithms. These approaches can estimate the uncertainty of their answers and provide theoretical guarantees of correctness, but can only leverage explicitly defined regularizers and do not cope well with complex noise sources or missing data. Very recently, methods like Blush regularization in cryo-EM reconstruction [37] use a data-driven prior based on the noise2noise framework [42] to bypass the need for heuristic regularizers. However, the denoiser does not explicitly leverage the knowledge that proteins are made of atoms and cannot take advantage of a known amino acid sequence.

Recently, supervised-learning approaches have emerged as an alternative to the MAP framework and some of them established a new empirical state of the art for certain tasks. The algorithm

^{*}Correspondence to: axlevy@stanford.edu, gordon.wetzstein@stanford.edu

ModelAngelo [31], for example, can convert cryo-EM density maps into 3D atomic models with unprecedented accuracy. Typically, these supervised learning methods view the reconstruction problem as a regression task where a mapping between experimental measurements and atomic models needs to be learned. Some of these, like ModelAngelo, can even combine experimental data with sequence information by leveraging a pretrained protein language model [53]. However, these methods can only cope with a predefined type of input data. If additional information is available in a format that the model was not trained on (e.g., structural information about a fragment of the protein), or if the distribution of input data shifts at inference time (e.g., if the noise level changes due to modifications in the experimental protocol), a new model needs to be trained to properly cope with the new data.

In the field of imaging, scenarios where an image or a 3D model must be inferred from corrupted and partial observations are known as "inverse problems". To overcome the ill-posedness of these problems, regularizers were heuristically defined to inject hand-crafted priors and turn Maximum Likelihood Estimation (MLE) problems into MAP problems. In a similar fashion, machine learning-based methods were recently shown to outperform hand-crafted algorithms for a wide variety of tasks: denoising [74], inpainting [72], super-resolution [45], deblurring [49], monocular depth estimation [20], and camera calibration [36], among others. Recently, generative models were shown to be an effective way to inject data-driven priors into MAP problems, making inverse problems well-posed while replacing heuristic priors [6]. Among these generative methods, diffusion models gained popularity due to their powerful capabilities in the unconditional generation of images [19], videos [26], and 3D assets [51], and were recently leveraged to solve inverse problems in image space [59, 10].

The field of structural biology has also witnessed the application of diffusion models in protein structure modeling tasks [70, 1]. Building on recent progress in protein structure prediction [33] (sequence to structure) and fixed-backbone design [3] (structure to sequence), these diffusion models have opened the doors to *de novo* protein design [28, 70, 2, 73] (joint generation of structure and sequence). In particular, the recently released generative model Chroma [29] stands out in part thanks to its "programmable" framework, i.e. its ability to be conditioned on external hard or soft constraints. However, despite experimentally validated state-of-the-art results at unconditional generation and its programmable framework, Chroma has not yet been applied to inverse problems like atomic model building.

Here, we introduce ADP-3D (Atomic Denoising Prior for 3D reconstruction), a framework to condition a diffusion model in protein space with any observations for which the measurement process can be physically modeled. Instead of using unadjusted Langevin dynamics for posterior sampling, our approach performs MAP estimation and leverages the data-driven prior learned by a diffusion model using the plug-n-play framework [67]. We demonstrate that our method handles a variety of external information: simulated cryo-EM density maps, amino acid sequence, partial 3D structure, and pairwise distances between amino acid residues, to refine a complete 3D atomic model of the protein. We show that our method outperforms posterior sampling baselines and, given a cryo-EM density map, can accurately refine incomplete atomic models provided by Modelangelo. In all our experiments, we use Chroma [29] as our pretrained generative model and highlight the importance of the diffusion-based prior. We therefore make the following contributions:

- We introduce a versatile framework, inspired from plug-n-play, to solve inverse problems in protein space with a pretrained diffusion model as a learned prior;
- We outperform existing posterior sampling methods at reconstructing full protein structures from partial structures;
- We show that a protein diffusion model can be guided to perform atomic model refinement in simulated cryo-EM density maps;
- We show that a protein diffusion model can be conditioned on a sparse distance matrix.

2 Related Work

Protein Diffusion Models. Considerable progress has been made in leveraging diffusion models for protein structure generation. Lee et al. [41] demonstrated *de novo* protein generation using diffusion models over 2D distance matrices, requiring a post-processing step to produce 3D structures.

Conditioned on secondary structure adjacency matrices, Anand and Achim [2] used a 3D point cloud representation to generate new structures. Trippe et al. [66] circumvented the need for conditioning information, demonstrated unconditional generation of proteins larger than 20 amino acid residues and introduced a novel conditional sampling algorithm to generate structures respecting a target motif. Wu et al. [71] built a generative model that directly operates on backbone internal coordinates (i.e., dihedral angles), thereby ensuring SE(3)-equivariance. Based on theoretical works extending diffusion models to Riemannian manifolds [16, 40], Yim et al. [73] introduced a principled formulation of diffusion models in SE(3) and represented protein backbones as elements of $SE(3)^N$. In RFdiffusion, Watson et al. [70] experimentally designed the generated proteins and structurally validated them with cryo-EM. Recently, AlphaFold 3 [1] showed that a diffusion model operating on raw atom coordinates could be used as a tool to improve protein structure prediction. Diffusion models have been used to address specific tasks in protein space, like the generation of complementarity-determining region (CDR)-loops conditioned on non-CDR regions of antibody-antigen complexes [47], or sequence-to-structure prediction [32].

Out of the existing generative models for proteins, Chroma [29] has reported state-of-the-art "designability" metrics with a model that can be conditioned to generate proteins with desired properties (e.g., substructure motifs, symmetries). Despite its modular interface in which users can define their own *conditioners*, Chroma has not yet been used to guide the generative model with experimental measurements and solve real-world inverse problems. Here, we introduce a framework to efficiently condition a pretrained protein diffusion model and demonstrate the possibility of using cryo-EM maps as conditioning information.

Diffusion-Based Posterior Sampling in Image Space. An *inverse problem* in image space can be defined by $\mathbf{y} = \Gamma(\mathbf{x}) + \eta$ where \mathbf{x} is an unknown image, \mathbf{y} a measurement, Γ a known operator and η a noise vector of known distribution, potentially signal-dependent. The goal of posterior sampling is to sample \mathbf{x} from the posterior $p(\mathbf{x}|\mathbf{y})$, the normalized product of the prior $p(\mathbf{x})$ and the likelihood $p(\mathbf{y}|\mathbf{x})$. Bora et al. [6] showed that generative models could be leveraged to implicitly represent a data-learned prior and solve compressed sensing problems in image space. Motivated by the success of diffusion models at unconditional generation [19], several works showed that score-based and denoising models could be used to solve linear inverse problems like super-resolution, deblurring, inpainting and colorization [43, 8, 55, 35, 46, 76], leading to results of unprecedented quality. Other methods leveraged the score learned by a diffusion model to solve inverse problems in medical imaging [60, 30, 9, 12, 11] and astronomy [61]. Finally, recent methods went beyond the scope of linear problems and used diffusion-based posterior sampling on nonlinear problems like JPEG restoration [59], phase retrieval and non-uniform deblurring [10]. Taking inspiration from these methods, we propose to leverage protein diffusion models to solve nonlinear inverse problems in protein space.

Model Building Methods. Cryogenic electron-microscopy (cryo-EM) provides an estimate of the 3D electron scattering potential (or density map) of a protein. The task of fitting an atomic model \mathbf{x} into this 3D map \mathbf{y} is called model building and can be seen as a nonlinear inverse problem in protein space (see 4.3).

Model building methods were first developed in X-Ray crystallography [13] and automated methods like Rosetta *de-novo* [68], PHENIX [44, 65] and MAINMAST [64] were later implemented for cryo-EM data. Although they constituted a milestone towards the automation of model building, obtained structures were often incomplete and needed refinement [58]. Supervised learning techniques were built for model building, relying on CNN and U-Net-based architectures [57, 75, 50]. EMBuild [25] was the first method to make use of sequence information and Modelangelo [31] established a new state of the art for automated *de novo* model building. Trained on 3,715 experimental paired datapoints, Modelangelo uses a GNN-based architecture and processes the sequence information with a pretrained language model [53]. Although fully-supervised methods outperform previous approaches, they still provide incomplete atomic models and cannot use a type of input data it was not trained with as additional information.

Here, we propose a versatile framework to solve inverse problems in protein space, including atomic model refinement. Our approach can cope with auxiliary measurements for which the measurement process is known. Our framework allows any pretrained diffusion model to be plugged-in as a

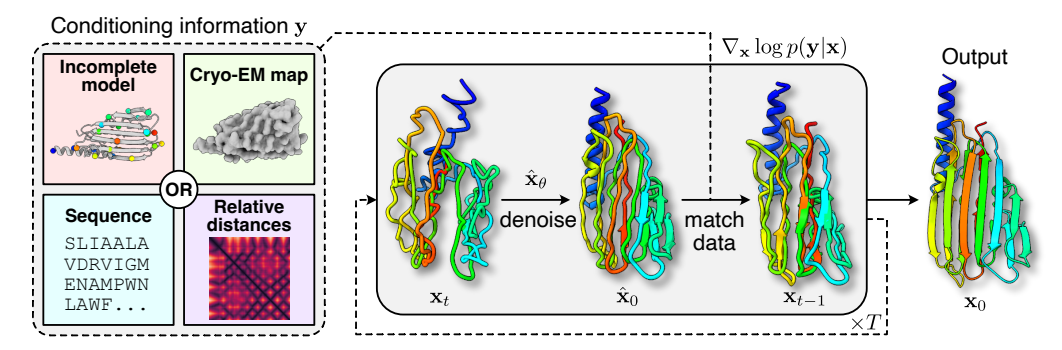


Figure 1: Overview of ADP-3D. Our method turns partial and noisy measurements (the "conditioning information") into a 3D structure by leveraging a pretrained diffusion model (here, Chroma [29]) and physics-based models of the measurement processes. Starting from a random structure \mathbf{x}_T , our method iterates between a denoising step and a data-matching step. The denoiser comes from the pretrained diffusion model. The data-matching step aims at maximizing the likelihood of the measurements.

prior and can therefore take advantage of future developments in generative models without any task-specific retraining step.

3 Background

3.1 Diffusion in Protein Space

We describe the atomic structure of a protein of N amino acid residues by the 3D Cartesian coordinates $\mathbf{x} \in \mathbb{R}^{4N \times 3}$ of the four backbone heavy atoms (N, C_{α}, C, O) in each residue, the amino acid sequence $\mathbf{s} \in \{1,...,20\}^N$, and the side chain torsion angles for each amino acid $\chi \in (-\pi,\pi]^{4N}$ (the conformation of the side chain can be factorized as up to four sequential rotations).

In Chroma [29], the joint distribution over all-atom structures is factorized as

$$p(\mathbf{x}, \mathbf{s}, \chi) = p(\mathbf{x})p(\mathbf{s}|\mathbf{x})p(\chi|\mathbf{x}, \mathbf{s}). \tag{1}$$

The first factor on the right hand side, $p(\mathbf{x})$, is modeled as a diffusion process operating in the space of backbone structures \mathbf{x} . Given a structure \mathbf{x} at diffusion time t, Chroma models the conditional distribution of the sequence $p_{\theta}(\mathbf{s}|\mathbf{x},t)$ as a conditional random field and the conditional distribution of the side chain conformations $p_{\theta}(\mathbf{x}|\mathbf{x},\mathbf{s},t)$ with an autoregressive model.

Adding isotropic Gaussian noise to a backbone structure would rapidly destroy simple biophysical patterns that proteins always follow (e.g., the scaling law of the radius of gyration with the number of residues). Instead, Chroma uses a non-isotropic noising process as an inductive bias to alleviate the need for the model to learn these patterns from the data. The correlation of the noise is defined in such a way that a few structural properties are statistically preserved throughout the noising process. Specifically, the forward diffusion process is defined by the variance preserving stochastic process

$$d\mathbf{x} = -\frac{1}{2}\mathbf{x}\beta_t dt + \sqrt{\beta_t}\mathbf{R}d\mathbf{w},$$
(2)

where β_t is a time-dependent noising schedule and dw is a standard Wiener process of dimension $\mathbb{R}^{4N\times3}$. The matrix $\mathbf{R}\in\mathbb{R}^{4N\times4N}$ is fixed and defined explicitly based on statistical considerations regarding the structure of proteins (see [29] and supplementary). Starting from \mathbf{x}_0 at t=0, a solution to this stochastic differential equation (SDE) at time t is given by

$$\mathbf{x}_t \sim \mathcal{N}(\mathbf{x}; \alpha_t \mathbf{x}_0, \sigma_t^2 \mathbf{R} \mathbf{R}^T),$$
 (3)

where
$$\alpha_t = \exp\left(-\frac{1}{2} \int_0^t \beta_s ds\right)$$
 and $\sigma_t = \sqrt{1 - \alpha_t^2}$.

New protein samples can be generated by sampling \mathbf{x}_T from $\mathcal{N}(0, \mathbf{R}\mathbf{R}^T)$ and integrating the following reverse-time SDE over $t \in [T, 0]$ [4]:

$$d\mathbf{x} = \left[-\frac{1}{2} \mathbf{x} - \mathbf{R} \mathbf{R}^T \nabla_{\mathbf{x}} \log p_t(\mathbf{x}) \right] \beta_t dt + \sqrt{\beta_t} \mathbf{R} d\bar{\mathbf{w}}, \tag{4}$$

where $d\bar{\mathbf{w}}$ is a reverse-time Wiener process. Following Tweedie's formula [54], the score $\nabla_{\mathbf{x}} \log p_t(\mathbf{x})$ is an affine function of the time-dependent *optimal denoiser*, approximated by $\hat{\mathbf{x}}_{\theta}(\mathbf{x}, t)$:

$$\nabla_{\mathbf{x}} \log p_t(\mathbf{x}) = \frac{(\mathbf{R}\mathbf{R}^T)^{-1}}{1 - \alpha_t^2} (\alpha_t \mathbb{E}[\mathbf{x}_0 | \mathbf{x}_t = \mathbf{x}] - \mathbf{x}), \quad \hat{\mathbf{x}}_{\theta}(\mathbf{x}, t) \approx \mathbb{E}[\mathbf{x}_0 | \mathbf{x}_t = \mathbf{x}].$$
 (5)

In practice, the SDE (4) is modified with a low-temperature sampling strategy in order to promote high-likelihoood states. The reverse-time low-temperature diffusion process is equilibrated with Langevin dynamics and solved numerically with the Euler-Maruyama method.

3.2 Half Quadratic Splitting and Plug-n-Play Framework

An objective function of the form $f(\mathbf{x}) + g(\mathbf{x})$ can be efficiently minimized over \mathbf{x} using a variable splitting algorithm like Half Quadratic Splitting (HQS) [23]. By introducing an auxiliary variable $\tilde{\mathbf{x}}$, the HQS method relies on iteratively solving two subproblems:

$$\tilde{\mathbf{x}}_{k} = \operatorname{prox}_{g,\rho}(\mathbf{x}_{k}) = \underset{\tilde{\mathbf{x}}}{\operatorname{argmin}} g(\tilde{\mathbf{x}}) + \frac{\rho}{2} \|\tilde{\mathbf{x}} - \mathbf{x}_{k}\|_{2}^{2},
\mathbf{x}_{k+1} = \operatorname{prox}_{f,\rho}(\tilde{\mathbf{x}}_{k}) = \underset{\tilde{\mathbf{x}}}{\operatorname{argmin}} f(\mathbf{x}) + \frac{\rho}{2} \|\mathbf{x} - \tilde{\mathbf{x}}_{k}\|_{2}^{2},$$
(6)

where prox are called "proximal operators" and $\rho > 0$ is a user-defined proximal parameter.

If f represents a negative log-likelihood over $\mathbf x$ and g represents a negative log-prior, the above problem defines a Maximum-A-Posterior (MAP) problem. The key idea of the plug-and-play framework [67] is to notice that the first minimization problem in (6) is exactly a Gaussian denoising problem at noise level $\sigma = \sqrt{1/\rho}$ with the prior $\exp(-g(\mathbf x))$ in $\mathbf x$ -space. This means that any Gaussian denoiser can be used to "plug in" a prior into a MAP problem.

Once a diffusion model has been trained, it provides a deterministic Gaussian denoiser for various noise levels, as described in (5). As recently shown in Zhu et al. [76], this optimal denoiser can be used in the plug-n-play framework to solve MAP problems in image space. Here, we propose to apply this idea to inverse problems in protein space, leveraging a pretrained diffusion model.

4 Methods

In this section, we formulate our method, ADP-3D (Atomic Denoising Prior for 3D reconstruction), as a MAP estimation method in protein space and explain how the plug-n-play framework can be used to leverage the prior learned by a pretrained diffusion model. We then introduce our preconditioning strategy in the case of linear problems. Finally, we describe and model the measurement process in cryogenic electron microscopy. ADP-3D is described with pseudo-code in Algorithm 1.

4.1 General Approach

Given a set of independent measurements $\mathbf{Y} = \{\mathbf{y}_i\}_{i=1}^n$ made from the same unknown protein, our goal is to find a Maximum-A-Posteriori (MAP) estimate of the backbone structure \mathbf{x}^* . Following Bayes' rule,

$$\mathbf{x}^* = \underset{\mathbf{x}}{\operatorname{argmax}} \left\{ p_0(\mathbf{x}|\mathbf{Y}) \right\} = \underset{\mathbf{x}}{\operatorname{argmin}} \left\{ \underbrace{-\sum_{i=1}^n \log p_0(\mathbf{y}_i|\mathbf{x})}_{f(\mathbf{x})} \underbrace{-\log p_0(\mathbf{x})}_{g(\mathbf{x})} \right\}. \tag{7}$$

While most of previous works leveraging a diffusion model for inverse problems aim at sampling from the posterior distribution $p(\mathbf{x}|\mathbf{Y})$, we are interested here in scenarios where the measurements convey enough information to make the MAP estimate unique and well-defined. In the results section, we show that MAP estimation outperforms posterior sampling in such well-defined problems.

We take inspiration from the plug-and-play framework [67] to efficiently solve (7). We propose to use the optimal denoiser $\hat{\mathbf{x}}_{\theta}(\mathbf{x},t)$ of a pretrained diffusion model to solve the first subproblem in (6). Framing the optimization loop in the whitened space of $\mathbf{z} = \mathbf{R}^{-1}\mathbf{x}$, which provides more stable

Algorithm 1 ADP-3D (Atomic Denoising Prior for 3D reconstruction)

```
Inputs: log-likelihood functions \{f_i: (\mathbf{y}, \mathbf{z}) \mapsto \log p(\mathbf{y}_i = \mathbf{y}|\mathbf{z})\}_{i=1}^n, measurements \{\mathbf{y}_i\}. Diffusion model: correlation matrix \mathbf{R}, denoiser \hat{\mathbf{x}}_{\theta}(\mathbf{x}, t), schedule \{\alpha_t\}_{t=1}^T. Optimization parameters: learning rates \{\lambda_i\}, momenta \{\rho_i\}. Initialization: \mathbf{z}_T \leftarrow \mathcal{N}(0, \mathbf{I}), \quad \forall i, \mathbf{v}_i = 0 for t = T, \dots, 1 do  \tilde{\mathbf{z}}_0 \leftarrow \mathbf{R}^{-1}\hat{\mathbf{x}}_{\theta}(\mathbf{R}\mathbf{z}_t, t) \qquad \qquad \text{Denoise at level } t \\ \forall i, \mathbf{v}_i = \rho_i \mathbf{v}_i + \lambda_i \nabla_{\mathbf{z}} f_i(\mathbf{y}_i, \mathbf{z})|_{\mathbf{z} = \tilde{\mathbf{z}}_0} \qquad \qquad \text{Accumulate gradient of log likelihood} \\ \tilde{\mathbf{z}}_0 \leftarrow \tilde{\mathbf{z}}_0 + \sum_i \mathbf{v}_i \qquad \qquad \qquad \text{Take a step to maximize likelihood} \\ \mathbf{z}_{t-1} \sim \mathcal{N}(\alpha_{t-1}\hat{\mathbf{z}}_0, \sigma_{t-1}^2) \qquad \qquad \qquad \text{Add noise at level } t-1 \\ \text{end for} \\ \text{return } \mathbf{x}_0 = \mathbf{R}\mathbf{z}_0
```

results, our general optimization algorithm can be summarized in three steps:

$$\begin{split} \tilde{\mathbf{z}}_0 &= \mathbf{R}^{-1} \hat{\mathbf{x}}_{\theta}(\mathbf{R}\mathbf{z}_t, t) & \text{Denoise at level } t, \\ \hat{\mathbf{z}}_0 &= \underset{\mathbf{z}}{\operatorname{argmin}} \frac{\rho}{2} \|\mathbf{z} - \tilde{\mathbf{z}}_0\|_2^2 - \sum_{i=1}^n \log p_0(\mathbf{y}_i | \mathbf{z}) & \text{Maximize likelihood,} \\ \mathbf{z}_{t-1} &\sim \mathcal{N}(\alpha_{t-1}\hat{\mathbf{z}}_0, \sigma_{t-1}^2) & \text{Add noise at level } t-1. \end{split}$$

Here, no specific assumptions have been made on the likelihood term and this framework could hypothetically be applied on any set of measurements for which we have a physics-based model of the measurement process. Since the second step is not tractable in most cases, we replace the explicit minimization with a gradient step with momentum from the iterate $\tilde{\mathbf{z}}_0$. This step can be implemented efficiently using automatic differentiation.

4.2 Preconditioning for Linear Measurements

We consider the case where the measurement process is linear:

$$\mathbf{y} = \mathbf{A}\mathbf{x}_0 + \eta = \mathbf{A}\mathbf{R}\mathbf{z}_0 + \eta, \quad \eta \sim \mathcal{N}(0, \Sigma \in \mathbb{R}^{m \times m}),$$
 (8)

with $\mathbf{y} \in \mathbb{R}^m$ and $\mathbf{A} \in \mathbb{R}^{m \times 4N}$ being a known measurement matrix of rank m. In this case, the log-likelihood term is a quadratic function:

$$\log p_0(\mathbf{y}|\mathbf{z}) = -\frac{1}{2} \|\mathbf{A}\mathbf{R}\mathbf{z} - \mathbf{y}\|_{\mathbf{\Sigma}^{-1}}^2 + C, \text{ where } \|\mathbf{x}\|_{\mathbf{\Sigma}^{-1}}^2 = \mathbf{x}^T \mathbf{\Sigma}^{-1} \mathbf{x},$$
(9)

and C does not depend on \mathbf{z} . As shown in Figure 2, the condition number of \mathbf{R} (i.e., the ratio between its largest and smallest singular values) grows as a power function of the number of residues. For typical proteins ($N \geq 100$), this condition number exceeds 100, making the maximization of the above term an ill-conditioned problem. In order to make gradient-based optimization more efficient, we propose to $\operatorname{precondition}$ the problem by precomputing a singular value decomposition $\mathbf{A}\mathbf{R} = \mathbf{U}\mathbf{S}\mathbf{V}^T$ and to set $\mathbf{\Sigma} = \sigma^2\mathbf{U}\mathbf{S}\mathbf{S}^T\mathbf{U}^T$. Note that this is equivalent to modeling the measurement process as $\mathbf{y} = \mathbf{A}\mathbf{R}(\mathbf{z} + \tilde{\eta})$ with $\tilde{\eta} \sim \mathcal{N}(0, \sigma^2)$. In other words, we assume that the noise η preserves the simple patterns in proteins, which is a reasonable hypothesis if, for example, \mathbf{y} is an incomplete atomic model obtained by an upstream reconstruction algorithm that leverages prior knowledge on protein structures. The log-likelihood then becomes

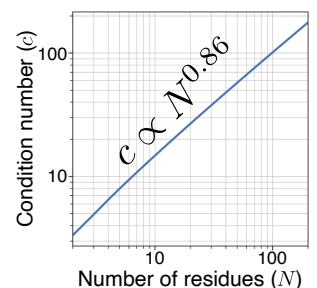


Figure 2: Condition number of \mathbf{R} vs. number of residues N.

$$\log p_0(\mathbf{y}|\mathbf{z}) = -\frac{1}{2\sigma^2} \left\| \begin{pmatrix} \mathbf{I}_m & 0\\ 0 & 0 \end{pmatrix} \mathbf{V}^T \mathbf{z} - \mathbf{S}^+ \mathbf{U}^T \mathbf{y} \right\|_2^2 + C.$$
 (10)

The maximization of this term is a well-posed problem that gradient ascent with momentum efficiently solves (see supplementary analyses). In (10), S^+ denotes the pseudo-inverse of S.

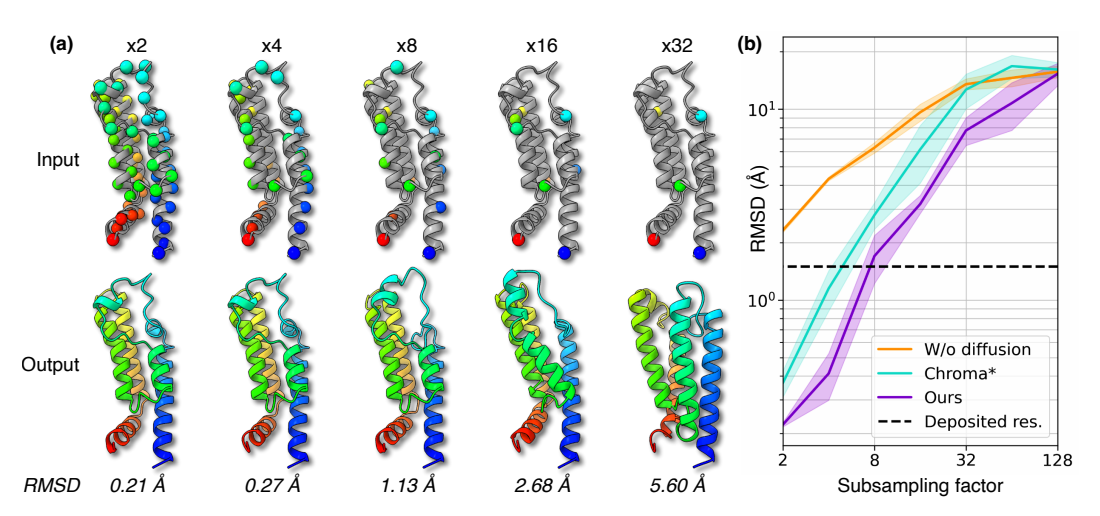


Figure 3: Structure Completion. Results on the ATAD2 protein (PDB:7qum, 130 residues). (a) Qualitative results. The input structure is a subsampled version of the target structure (subsampling factor in the top row). In the "input" row, we show the target (unknown) in gray and the locations of the known alpha carbons in colors. We report the lowest RMSD over 8 runs. (b) RMSD vs. subsampling factor. Our method is compared to Chroma conditioned with the SubstructureConditioner. The importance of the diffusion-based prior is shown. We report the mean RMSD (±1 std) over 8 runs. The experimental (deposited) resolution is indicated with a dashed line.

4.3 Application to Atomic Model Building

Measurement Model in Cryo-EM. In single particle cryo-EM, a purified solution of a target protein is flash-frozen and imaged with a transmission electron microscope, providing thousands to millions of randomly oriented 2D projection images of the protein's electron scattering potential. Reconstruction algorithms process these images and infer a 3D *density map* of the protein. Given a protein $(\mathbf{x}, \mathbf{s}, \chi)$, its density map is well approximated by [17]

$$\mathbf{y} = \mathcal{B}(\Gamma(\mathbf{x}, \mathbf{s}, \chi)) + \eta \in \mathbb{R}^{D \times D \times D},\tag{11}$$

where Γ is an operator that places a sum of 5 isotropic Gaussians centered on each heavy atom. The amplitudes and standard deviations of these Gaussians, known as "form factors", are tabulated [24] and depend on the chemical element they are centered on. \mathcal{B} represents the effect of "B-factors" [34] and can be viewed as a spatially-dependent blurring kernel modelling molecular motions and/or signal damping by the transfer function of the electron microscope. η models isotropic Gaussian noise of variance σ^2 . This measurement model leads to the following log-likelihood:

$$\log p_0(\mathbf{y}|\mathbf{x}, \mathbf{s}, \chi) = -\frac{1}{2\sigma^2} \|\mathbf{y} - \mathcal{B}(\Gamma(\mathbf{x}, \mathbf{s}, \chi))\|_2^2 + C.$$
 (12)

Likelihood Terms in Model Refinement. We consider a 3D density map \mathbf{y} provided by an upstream reconstruction method and an incomplete backbone structure $\bar{\mathbf{x}} \in \mathbb{R}^m$ ($m \le 4N$) provided by an upstream model building algorithm (e.g., ModelAngelo [31]). Sequencing a protein is now a routine process [18] and we therefore consider the sequence \mathbf{s} as an additional source of information. The side chain angles χ are, however, unknown.

The log-likelihood of our measurements for a given backbone structure x can be decomposed as

$$\log p_0(\mathbf{y}, \mathbf{s}, \bar{\mathbf{x}} | \mathbf{x}) = \log p_0(\mathbf{s} | \mathbf{x}) + \log p_0(\bar{\mathbf{x}} | \mathbf{x}) + \log p_0(\mathbf{y} | \mathbf{x}, \mathbf{s}). \tag{13}$$

On the right-hand side, the first term can be approximated using the learned conditional distribution $p_{\theta}(\mathbf{s}|\mathbf{x},t=0)$. We model $\bar{\mathbf{x}} = \mathbf{M}\mathbf{x} + \eta$ so that the second term can be handled by the preconditioning procedure described in the previous section. Finally, the last term involves the marginalization of $p_0(\mathbf{y}|\mathbf{x},\mathbf{s},\chi)$ over χ . This marginalization is not tractable but (12) provides a lower bound:

$$\log p_0(\mathbf{y}|\mathbf{x}, \mathbf{s}) \ge \mathbb{E}_{\chi \sim p_0(\chi|\mathbf{x}, \mathbf{s})} \Big[\log p_0(\mathbf{y}|\mathbf{x}, \mathbf{s}, \chi) \Big] \approx \mathbb{E}_{\chi \sim p_\theta(\chi|\mathbf{x}, \mathbf{s}, t = 0)} \Big[\log p_0(\mathbf{y}|\mathbf{x}, \mathbf{s}, \chi) \Big], \quad (14)$$

using Jensen's inequality. The expectation is approximated by Monte Carlo sampling and gradients of χ with respect to \mathbf{x} are computed by automatic differentiation through the autoregressive sampler of χ .

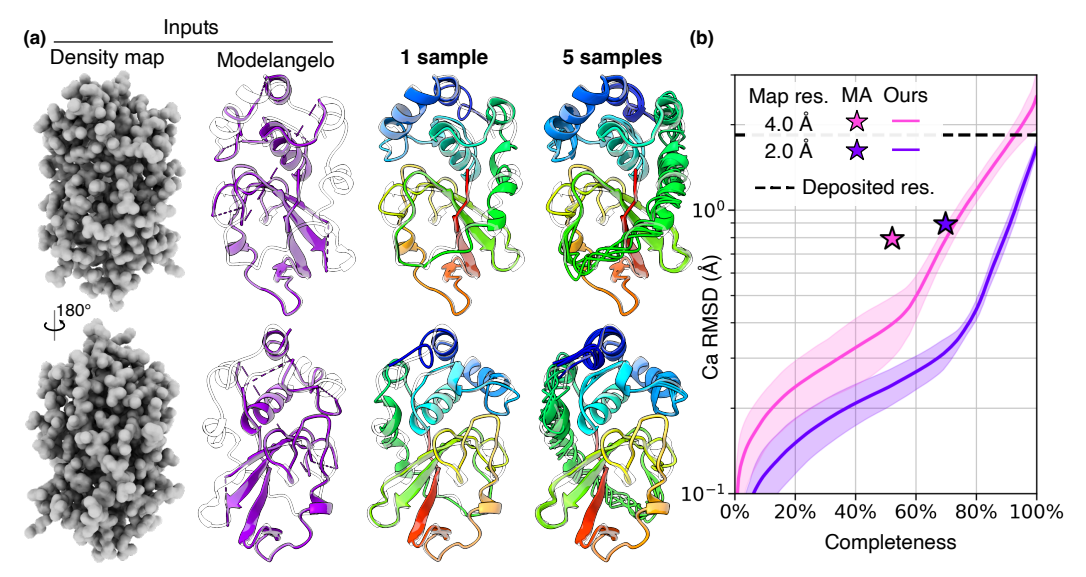


Figure 4: Atomic Model Refinement. Results on the TecA bacterial toxin (PDB:7pzt, 160 residues). (a) Qualitative results. From left to right: the input density map at 2.0 Å resolution, the incomplete model given by ModelAngelo and our refined models (1 sample and 5 samples), overlaid on the target structure in transparency. (b) RMSD of alpha carbons vs. completeness (number of predicted residues / total number of residues) with ModelAngelo (MA) and our method. We run 5 experiments and report the mean of the lowest RMSD on α -carbons over 8 replicas (± 1 std). The experimental (deposited) resolution is indicated with a dashed line.

5 Experiments

Experimental Setup. Our method uses the publicly released version of Chroma² [29]. We run all our experiments using structures of proteins downloaded from the Protein Data Bank (PDB) [7]. In order to select proteins that do not belong to the training dataset of Chroma, here we only consider structures that were released after 2022-03-20 (Chroma was trained on a filtered version of the PDB queried on that date). We only consider single-chain structures for which all the residues have been spatially resolved, so that the Root Mean Square Deviation (RMSD) of the predicted Cartesian coordinates can be computed for all the heavy atoms in the backbone. In each experiment, we run 8 replicas in parallel on a single NVIDIA A100 GPU.

Structure Completion. Given an incomplete atomic model of a protein, our first task is to predict the coordinates of all heavy atoms in the backbone. The forward measurement process can be modeled as $\mathbf{y} = \mathbf{M}\mathbf{x}$ where $\mathbf{M} \in \{0,1\}^{(4N/k)\times 4N}$ is a *masking* matrix $(\mathbf{M}\mathbf{1} = \mathbf{1})$ and k is the *subsampling factor*. We consider the case where, for each residue, the location of all 4 heavy atoms on the backbone $(\mathbf{N}, \mathbf{C}_{\alpha}, \mathbf{C}, \mathbf{O})$ is either known or unknown. Residues of known locations are regularly spaced along the backbone every k residues. We compare our results to the baseline Chroma conditioned with a SubstructureConditioner [29]. This baseline samples from the posterior probability $p(\mathbf{x}|\mathbf{y})$ using unadjusted Langevin dynamics. We use 1000 diffusion steps for our method and the baseline.

In Figure 3, we show our results on ATAD2 (PDB:7qum) [15, 5], a cancer-associated protein of 130 residues. The protein was resolved at a resolution of 1.5 Å using X-ray crystallography. Our method recovers the target structure without loss of information (RMSD < 1.5 Å) for subsampling factors of 2, 4 and 8. Fig. 3.b shows that our method outperforms the baseline and highlights the importance of the diffusion-based prior. When the subsampling factor is large (≥ 32), the reconstruction accuracy decreases but the method inpaints unknown regions with realistic secondary structures (see quantitative evaluation in the supplementary). Note that making the conditioning information sparser (increasing the subsampling factor) tends to close the gap between our method (MAP estimation) and the baseline (posterior sampling). We provide results on four other protein structures in the supplementary.

Atomic Model Refinement. Next, we evaluate our method on the model refinement task. We use ChimeraX [48, 62] to simulate the 3D density maps of a single-chain protein, at different resolutions. We run the state-of-the-art model building method ModelAngelo [31] on the simulated maps, using

²https://github.com/generatebio/chroma

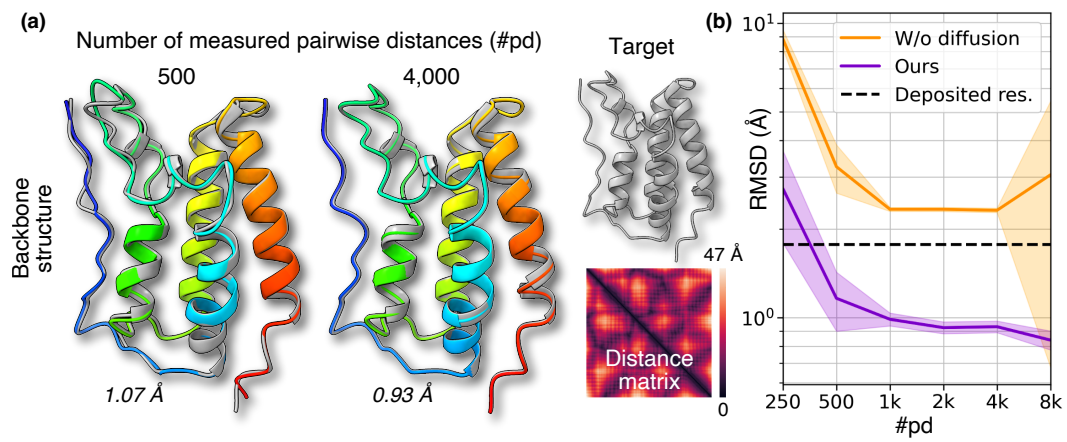


Figure 5: Pairwise Distances to Structures. Results on BRD4 (PDB: 7r5b, 127 residues) (a) Qualitative results. The reconstructed structures are shown in colors, depending on the number of known pairwise distances. We report the lowest RMSD over 8 runs. The target structure is shown in gray along with its pairwise distance matrix. (b) RMSD vs. number of known pairwise distances. Each experiment is ran 10 times with randomly sampled distances. We report the mean of the lowest RMSD obtained over 8 replicas (±1 std). The plot demonstrates the importance of the diffusion model. The experimental (deposited) resolution is indicated with a dashed line.

the known sequence. Then, we provide ModelAngelo's output (an incomplete model) to our method, along with the density map and the sequence. We use ModelAngelo's default parameters. To evaluate our method, we report the RMSD of the predicted structure for the X% most well-resolved alpha carbons (compared to the deposited structure), for $X \in [0, 100]$ (X is called the "completeness").

In Figure 4, we show our results on a synthetic density map of the TecA bacterial toxin (PDB:7pzt). This protein structure belongs to the CASP15 dataset, released in May 2022 to evaluate protein structure modeling methods. Proteins belonging to this dataset were selected for not having close homologous in the PDB, which ensures that Chroma was not trained on similar structures. The protein was resolved at 1.84 Å resolution using X-ray crystallography. Note that we do not chose a structure that was resolved with cryo-EM because most cryo-EM-resolved models are incomplete. For both input resolutions (2.0 Å and 4.0 Å), our method improves on ModelAngelo's accuracy for a fixed completeness level (and reaches a higher completeness for the same accuracy). We explore the effect of removing some of the conditioning information in the supplementary materials.

Pairwise Distances to Structure Finally, we assume we are given a set of pairwise distances between alpha carbons of a protein and we use our method to predict a full 3D structure. This task is a simplification of the reconstruction problem in paramagnetic NMR spectroscopy, where one can obtain information about the relative distances and orientations between pairs of atoms via the nuclear Overhauser effect and sparse paramagnetic restraints, and must deduce the Cartesian coordinates of every atom [38, 39]. Formally, our measurement model is $\mathbf{y} = \|\mathbf{D}\mathbf{x}\|_2 \in \mathbb{R}^m$, where $\mathbf{D} \in \{-1,0,1\}^{m\times 4N}$ is the *distance matrix* and the norm is taken row-wise (in xyz space). \mathbf{D} contains a single "1" and a single "-1" in each row and is not redundant (the distance between a given pair of atoms is measured at most once). m corresponds to the number of measured distances.

We evaluate our method on the bromodomain-containing protein 4 (BRD4, PDB: 7r5b [69]), a protein involved in the development of a specific type of cancer (NUT midline carinoma) [22] and targeted by pharmaceutical drugs [14]. For a given number m, we randomly sample m pairs of alpha carbons (without redundancy) between which we assume the distances to be known. Our results are shown in Figure 5. When 500 pairwise distances or more are known, our method recovers the structural information of the target structure (RMSD < 1.77 Å, the resolution of the deposited structure resolved with X-ray crystallography). We conduct the same experiment without the diffusion model and show a drop of accuracy, highlighting the importance of the generative prior. Note that, when the diffusion model is removed, increasing the number of measurements increases the number of local minimima in the objective function and can therefore hurt the reconstruction quality (plot in Fig. 5, orange curve, far-right part).

6 Discussion

This paper introduces ADP-3D, a method to leverage a pretrained protein diffusion model for protein structure determination. ADP-3D is not tied to a specific diffusion model and allows for any data-

driven denoisers to be plugged in as priors. Our method can therefore continually benefit from the development of more powerful or more specialized generative models.

We focused here on cases where the measurement process is simulated and perfectly known. Considering real experimental measurements (e.g., cryo-EM or NMR data) would raise complex and exciting challenges. In particular, we hope ADP-3D can serve as a precursor for reconstructing all-atom models directly from cryo-EM images, a key to turn empirical conformational distributions into thermodynamic information [21]. In cases where the measurement process cannot be faithfully modeled due to complex nonidealities, or when the measurement process is not differentiable, our framework reaches its boundaries. At the detriment of versatility, exploring the possibility of fine-tuning a pretrained diffusion model on paired data for conditional generation constitutes another promising avenue for future work.

Acknowledgements. The author(s) are pleased to acknowledge that the work reported on in this paper was substantially performed using the Princeton Research Computing resources at Princeton University which is a consortium of groups led by the Princeton Institute for Computational Science and Engineering (PICSciE) and Office of Information Technology's Research Computing. This material is based upon work supported by the National Science Foundation under award number 2303178 to SFK. Any opinions, findings, and conclusions or recommendations expressed in this material are those of the authors and do not necessarily reflect the views of the National Science Foundation.

We thank Mike Dunne and Jay Shenoy for their insightful feedback on this manuscript.

References

- [1] Josh Abramson, Jonas Adler, Jack Dunger, Richard Evans, Tim Green, Alexander Pritzel, Olaf Ronneberger, Lindsay Willmore, Andrew J Ballard, Joshua Bambrick, et al. Accurate structure prediction of biomolecular interactions with alphafold 3. *Nature*, pages 1–3, 2024.
- [2] Namrata Anand and Tudor Achim. Protein structure and sequence generation with equivariant denoising diffusion probabilistic models. *arXiv preprint arXiv:2205.15019*, 2022.
- [3] Namrata Anand, Raphael Eguchi, Irimpan I Mathews, Carla P Perez, Alexander Derry, Russ B Altman, and Po-Ssu Huang. Protein sequence design with a learned potential. *Nature communications*, 13(1):746, 2022.
- [4] Brian DO Anderson. Reverse-time diffusion equation models. *Stochastic Processes and their Applications*, 12(3):313–326, 1982.
- [5] Paul Bamborough, Chun-wa Chung, Emmanuel H Demont, Rebecca C Furze, Andrew J Bannister, Ka Hing Che, Hawa Diallo, Clement Douault, Paola Grandi, Tony Kouzarides, et al. A chemical probe for the atad2 bromodomain. *Angewandte Chemie*, 128(38):11554–11558, 2016.
- [6] Ashish Bora, Ajil Jalal, Eric Price, and Alexandros G Dimakis. Compressed sensing using generative models. In *International conference on machine learning*, pages 537–546. PMLR, 2017.
- [7] Stephen K Burley, Charmi Bhikadiya, Chunxiao Bi, Sebastian Bittrich, Li Chen, Gregg V Crichlow, Cole H Christie, Kenneth Dalenberg, Luigi Di Costanzo, Jose M Duarte, et al. Rcsb protein data bank: powerful new tools for exploring 3d structures of biological macromolecules for basic and applied research and education in fundamental biology, biomedicine, biotechnology, bioengineering and energy sciences. *Nucleic acids research*, 49(D1):D437–D451, 2021.
- [8] Jooyoung Choi, Sungwon Kim, Yonghyun Jeong, Youngjune Gwon, and Sungroh Yoon. Ilvr: Conditioning method for denoising diffusion probabilistic models. *arXiv preprint arXiv:2108.02938*, 2021.
- [9] Hyungjin Chung and Jong Chul Ye. Score-based diffusion models for accelerated mri. *Medical image analysis*, 80:102479, 2022.

- [10] Hyungjin Chung, Jeongsol Kim, Michael T Mccann, Marc L Klasky, and Jong Chul Ye. Diffusion posterior sampling for general noisy inverse problems. arXiv preprint arXiv:2209.14687, 2022.
- [11] Hyungjin Chung, Byeongsu Sim, Dohoon Ryu, and Jong Chul Ye. Improving diffusion models for inverse problems using manifold constraints. *Advances in Neural Information Processing Systems*, 35:25683–25696, 2022.
- [12] Hyungjin Chung, Byeongsu Sim, and Jong Chul Ye. Come-closer-diffuse-faster: Accelerating conditional diffusion models for inverse problems through stochastic contraction. In *Proceedings of the IEEE/CVF Conference on Computer Vision and Pattern Recognition*, pages 12413–12422, 2022.
- [13] Kevin Cowtan. The buccaneer software for automated model building. 1. tracing protein chains. *Acta crystallographica section D: biological crystallography*, 62(9):1002–1011, 2006.
- [14] David Da Costa, Angelo Agathanggelou, Timothy Perry, Victoria Weston, Eva Petermann, Anastasia Zlatanou, Ceri Oldreive, Wenbin Wei, Grant Stewart, Joanna Longman, et al. Bet inhibition as a single or combined therapeutic approach in primary paediatric b-precursor acute lymphoblastic leukaemia. *Blood cancer journal*, 3(7):e126–e126, 2013.
- [15] Gemma Davison, Mathew P Martin, Shannon Turberville, Selma Dormen, Richard Heath, Amy B Heptinstall, Marie Lawson, Duncan C Miller, Yi Min Ng, James N Sanderson, et al. Mapping ligand interactions of bromodomains brd4 and atad2 with fraglites and peplites-halogenated probes of druglike and peptide-like molecular interactions. *Journal of Medicinal Chemistry*, 65(22):15416–15432, 2022.
- [16] Valentin De Bortoli, Emile Mathieu, Michael Hutchinson, James Thornton, Yee Whye Teh, and Arnaud Doucet. Riemannian score-based generative modelling. Advances in Neural Information Processing Systems, 35:2406–2422, 2022.
- [17] Marc De Graef. *Introduction to conventional transmission electron microscopy*. Cambridge university press, 2003.
- [18] Edmond De Hoffmann and Vincent Stroobant. Mass spectrometry: principles and applications. John Wiley & Sons, 2007.
- [19] Prafulla Dhariwal and Alexander Nichol. Diffusion models beat gans on image synthesis. *Advances in neural information processing systems*, 34:8780–8794, 2021.
- [20] David Eigen, Christian Puhrsch, and Rob Fergus. Depth map prediction from a single image using a multi-scale deep network. *Advances in neural information processing systems*, 27, 2014.
- [21] Joachim Frank and Abbas Ourmazd. Continuous changes in structure mapped by manifold embedding of single-particle data in cryo-em. *Methods*, 100:61–67, 2016.
- [22] Christopher A French. Demystified molecular pathology of nut midline carcinomas. *Journal of clinical pathology*, 63(6):492–496, 2010.
- [23] Donald Geman and Chengda Yang. Nonlinear image recovery with half-quadratic regularization. *IEEE transactions on Image Processing*, 4(7):932–946, 1995.
- [24] Theo Hahn, Uri Shmueli, and JC Wilson Arthur. *International tables for crystallography*, volume 1. Reidel Dordrecht, 1983.
- [25] Jiahua He, Peicong Lin, Ji Chen, Hong Cao, and Sheng-You Huang. Model building of protein complexes from intermediate-resolution cryo-em maps with deep learning-guided automatic assembly. *Nature Communications*, 13(1):4066, 2022.
- [26] Jonathan Ho, William Chan, Chitwan Saharia, Jay Whang, Ruiqi Gao, Alexey Gritsenko, Diederik P Kingma, Ben Poole, Mohammad Norouzi, David J Fleet, et al. Imagen video: High definition video generation with diffusion models. *arXiv preprint arXiv:2210.02303*, 2022.
- [27] Liu Hong and Jinzhi Lei. Scaling law for the radius of gyration of proteins and its dependence on hydrophobicity. *Journal of Polymer Science Part B: Polymer Physics*, 47(2):207–214, 2009.

- [28] Po-Ssu Huang, Scott E Boyken, and David Baker. The coming of age of de novo protein design. *Nature*, 537(7620):320–327, 2016.
- [29] John B Ingraham, Max Baranov, Zak Costello, Karl W Barber, Wujie Wang, Ahmed Ismail, Vincent Frappier, Dana M Lord, Christopher Ng-Thow-Hing, Erik R Van Vlack, et al. Illuminating protein space with a programmable generative model. *Nature*, 623(7989):1070–1078, 2023.
- [30] Ajil Jalal, Marius Arvinte, Giannis Daras, Eric Price, Alexandros G Dimakis, and Jon Tamir. Robust compressed sensing mri with deep generative priors. Advances in Neural Information Processing Systems, 34:14938–14954, 2021.
- [31] Kiarash Jamali, Lukas Käll, Rui Zhang, Alan Brown, Dari Kimanius, and Sjors HW Scheres. Automated model building and protein identification in cryo-em maps. *Nature*, pages 1–2, 2024.
- [32] Bowen Jing, Ezra Erives, Peter Pao-Huang, Gabriele Corso, Bonnie Berger, and Tommi Jaakkola. Eigenfold: Generative protein structure prediction with diffusion models. *arXiv* preprint arXiv:2304.02198, 2023.
- [33] John Jumper, Richard Evans, Alexander Pritzel, Tim Green, Michael Figurnov, Olaf Ronneberger, Kathryn Tunyasuvunakool, Russ Bates, Augustin Žídek, Anna Potapenko, et al. Highly accurate protein structure prediction with alphafold. *Nature*, 596(7873):583–589, 2021.
- [34] Satinder Kaur, Josue Gomez-Blanco, Ahmad AZ Khalifa, Swathi Adinarayanan, Ruben Sanchez-Garcia, Daniel Wrapp, Jason S McLellan, Khanh Huy Bui, and Javier Vargas. Local computational methods to improve the interpretability and analysis of cryo-em maps. *Nature communications*, 12(1):1240, 2021.
- [35] Bahjat Kawar, Michael Elad, Stefano Ermon, and Jiaming Song. Denoising diffusion restoration models. Advances in Neural Information Processing Systems, 35:23593–23606, 2022.
- [36] Alex Kendall, Matthew Grimes, and Roberto Cipolla. Posenet: A convolutional network for real-time 6-dof camera relocalization. In *Proceedings of the IEEE international conference on computer vision*, pages 2938–2946, 2015.
- [37] Dari Kimanius, Kiarash Jamali, Max E Wilkinson, Sofia Lövestam, Vaithish Velazhahan, Takanori Nakane, and Sjors HW Scheres. Data-driven regularisation lowers the size barrier of cryo-em structure determination. *bioRxiv*, pages 2023–10, 2023.
- [38] Julia Koehler and Jens Meiler. Expanding the utility of nmr restraints with paramagnetic compounds: background and practical aspects. *Progress in nuclear magnetic resonance spectroscopy*, 59(4):360–389, 2011.
- [39] Georg Kuenze, Richard Bonneau, Julia Koehler Leman, and Jens Meiler. Integrative protein modeling in rosettanmr from sparse paramagnetic restraints. *Structure*, 27(11):1721–1734, 2019.
- [40] Adam Leach, Sebastian M Schmon, Matteo T Degiacomi, and Chris G Willcocks. Denoising diffusion probabilistic models on so (3) for rotational alignment. In *ICLR 2022 Workshop on Geometrical and Topological Representation Learning*, 2022.
- [41] Jin Sub Lee, Jisun Kim, and Philip M Kim. Proteinsgm: Score-based generative modeling for de novo protein design. *bioRxiv*, pages 2022–07, 2022.
- [42] Jaakko Lehtinen, Jacob Munkberg, Jon Hasselgren, Samuli Laine, Tero Karras, Miika Aittala, and Timo Aila. Noise2noise: Learning image restoration without clean data. *arXiv preprint arXiv:1803.04189*, 2018.
- [43] Haoying Li, Yifan Yang, Meng Chang, Shiqi Chen, Huajun Feng, Zhihai Xu, Qi Li, and Yueting Chen. Srdiff: Single image super-resolution with diffusion probabilistic models. *Neurocomputing*, 479:47–59, 2022.

- [44] Dorothee Liebschner, Pavel V Afonine, Matthew L Baker, Gábor Bunkóczi, Vincent B Chen, Tristan I Croll, Bradley Hintze, L-W Hung, Swati Jain, Airlie J McCoy, et al. Macromolecular structure determination using x-rays, neutrons and electrons: recent developments in phenix. Acta Crystallographica Section D: Structural Biology, 75(10):861–877, 2019.
- [45] Bee Lim, Sanghyun Son, Heewon Kim, Seungjun Nah, and Kyoung Mu Lee. Enhanced deep residual networks for single image super-resolution. In *Proceedings of the IEEE conference on computer vision and pattern recognition workshops*, pages 136–144, 2017.
- [46] Andreas Lugmayr, Martin Danelljan, Andres Romero, Fisher Yu, Radu Timofte, and Luc Van Gool. Repaint: Inpainting using denoising diffusion probabilistic models. In *Proceedings of the IEEE/CVF conference on computer vision and pattern recognition*, pages 11461–11471, 2022.
- [47] Shitong Luo, Yufeng Su, Xingang Peng, Sheng Wang, Jian Peng, and Jianzhu Ma. Antigen-specific antibody design and optimization with diffusion-based generative models for protein structures. *Advances in Neural Information Processing Systems*, 35:9754–9767, 2022.
- [48] Elaine C Meng, Thomas D Goddard, Eric F Pettersen, Greg S Couch, Zach J Pearson, John H Morris, and Thomas E Ferrin. Ucsf chimerax: Tools for structure building and analysis. *Protein Science*, 32(11):e4792, 2023.
- [49] Seungjun Nah, Tae Hyun Kim, and Kyoung Mu Lee. Deep multi-scale convolutional neural network for dynamic scene deblurring. In *Proceedings of the IEEE conference on computer vision and pattern recognition*, pages 3883–3891, 2017.
- [50] Jonas Pfab, Nhut Minh Phan, and Dong Si. Deeptracer for fast de novo cryo-em protein structure modeling and special studies on cov-related complexes. *Proceedings of the National Academy of Sciences*, 118(2):e2017525118, 2021.
- [51] Ryan Po, Wang Yifan, Vladislav Golyanik, Kfir Aberman, Jonathan T Barron, Amit H Bermano, Eric Ryan Chan, Tali Dekel, Aleksander Holynski, Angjoo Kanazawa, et al. State of the art on diffusion models for visual computing. *arXiv preprint arXiv:2310.07204*, 2023.
- [52] Ali Punjani, John L Rubinstein, David J Fleet, and Marcus A Brubaker. cryosparc: algorithms for rapid unsupervised cryo-em structure determination. *Nature methods*, 14(3):290–296, 2017.
- [53] Alexander Rives, Joshua Meier, Tom Sercu, Siddharth Goyal, Zeming Lin, Jason Liu, Demi Guo, Myle Ott, C Lawrence Zitnick, Jerry Ma, et al. Biological structure and function emerge from scaling unsupervised learning to 250 million protein sequences. *Proceedings of the National Academy of Sciences*, 118(15):e2016239118, 2021.
- [54] Herbert E Robbins. An empirical bayes approach to statistics. In *Breakthroughs in Statistics: Foundations and basic theory*, pages 388–394. Springer, 1992.
- [55] Chitwan Saharia, Jonathan Ho, William Chan, Tim Salimans, David J Fleet, and Mohammad Norouzi. Image super-resolution via iterative refinement. *IEEE transactions on pattern analysis and machine intelligence*, 45(4):4713–4726, 2022.
- [56] Sjors HW Scheres. Relion: implementation of a bayesian approach to cryo-em structure determination. *Journal of structural biology*, 180(3):519–530, 2012.
- [57] Dong Si, Spencer A Moritz, Jonas Pfab, Jie Hou, Renzhi Cao, Liguo Wang, Tianqi Wu, and Jianlin Cheng. Deep learning to predict protein backbone structure from high-resolution cryo-em density maps. *Scientific reports*, 10(1):4282, 2020.
- [58] Abhishek Singharoy, Ivan Teo, Ryan McGreevy, John E Stone, Jianhua Zhao, and Klaus Schulten. Molecular dynamics-based refinement and validation for sub-5 å cryo-electron microscopy maps. *Elife*, 5:e16105, 2016.
- [59] Jiaming Song, Arash Vahdat, Morteza Mardani, and Jan Kautz. Pseudoinverse-guided diffusion models for inverse problems. In *International Conference on Learning Representations*, 2022.

- [60] Yang Song, Liyue Shen, Lei Xing, and Stefano Ermon. Solving inverse problems in medical imaging with score-based generative models. *arXiv preprint arXiv:2111.08005*, 2021.
- [61] Yu Sun, Zihui Wu, Yifan Chen, Berthy T Feng, and Katherine L Bouman. Provable probabilistic imaging using score-based generative priors. arXiv preprint arXiv:2310.10835, 2023.
- [62] Guang Tang, Liwei Peng, Philip R Baldwin, Deepinder S Mann, Wen Jiang, Ian Rees, and Steven J Ludtke. Eman2: an extensible image processing suite for electron microscopy. *Journal of structural biology*, 157(1):38–46, 2007.
- [63] John J Tanner. Empirical power laws for the radii of gyration of protein oligomers. *Acta Crystallographica Section D: Structural Biology*, 72(10):1119–1129, 2016.
- [64] Genki Terashi and Daisuke Kihara. De novo main-chain modeling for em maps using mainmast. *Nature communications*, 9(1):1618, 2018.
- [65] Thomas C Terwilliger, Paul D Adams, Pavel V Afonine, and Oleg V Sobolev. A fully automatic method yielding initial models from high-resolution cryo-electron microscopy maps. *Nature* methods, 15(11):905–908, 2018.
- [66] Brian L Trippe, Jason Yim, Doug Tischer, David Baker, Tamara Broderick, Regina Barzilay, and Tommi Jaakkola. Diffusion probabilistic modeling of protein backbones in 3d for the motif-scaffolding problem. *arXiv* preprint arXiv:2206.04119, 2022.
- [67] Singanallur V Venkatakrishnan, Charles A Bouman, and Brendt Wohlberg. Plug-and-play priors for model based reconstruction. In 2013 IEEE global conference on signal and information processing, pages 945–948. IEEE, 2013.
- [68] Ray Yu-Ruei Wang, Mikhail Kudryashev, Xueming Li, Edward H Egelman, Marek Basler, Yifan Cheng, David Baker, and Frank DiMaio. De novo protein structure determination from near-atomic-resolution cryo-em maps. *Nature methods*, 12(4):335–338, 2015.
- [69] Robin Warstat, Mehrosh Pervaiz, Pierre Regenass, Marius Amann, Karin Schmidtkunz, Oliver Einsle, Manfred Jung, Bernhard Breit, Martin Hügle, and Stefan Günther. A novel pan-selective bromodomain inhibitor for epigenetic drug design. *European Journal of Medicinal Chemistry*, 249:115139, 2023.
- [70] Joseph L Watson, David Juergens, Nathaniel R Bennett, Brian L Trippe, Jason Yim, Helen E Eisenach, Woody Ahern, Andrew J Borst, Robert J Ragotte, Lukas F Milles, et al. De novo design of protein structure and function with rfdiffusion. *Nature*, 620(7976):1089–1100, 2023.
- [71] Kevin E Wu, Kevin K Yang, Rianne van den Berg, Sarah Alamdari, James Y Zou, Alex X Lu, and Ava P Amini. Protein structure generation via folding diffusion. *Nature Communications*, 15(1):1059, 2024.
- [72] Junyuan Xie, Linli Xu, and Enhong Chen. Image denoising and inpainting with deep neural networks. *Advances in neural information processing systems*, 25, 2012.
- [73] Jason Yim, Brian L Trippe, Valentin De Bortoli, Emile Mathieu, Arnaud Doucet, Regina Barzilay, and Tommi Jaakkola. Se (3) diffusion model with application to protein backbone generation. *arXiv* preprint arXiv:2302.02277, 2023.
- [74] Kai Zhang, Wangmeng Zuo, Yunjin Chen, Deyu Meng, and Lei Zhang. Beyond a gaussian denoiser: Residual learning of deep cnn for image denoising. *IEEE transactions on image processing*, 26(7):3142–3155, 2017.
- [75] Xi Zhang, Biao Zhang, Peter L Freddolino, and Yang Zhang. Cr-i-tasser: assemble protein structures from cryo-em density maps using deep convolutional neural networks. *Nature* methods, 19(2):195–204, 2022.
- [76] Yuanzhi Zhu, Kai Zhang, Jingyun Liang, Jiezhang Cao, Bihan Wen, Radu Timofte, and Luc Van Gool. Denoising diffusion models for plug-and-play image restoration. In *Proceedings* of the IEEE/CVF Conference on Computer Vision and Pattern Recognition, pages 1219–1229, 2023.

Appendix

A Log-Likelihood Functions

We define here the log-likelihood functions, as mentioned in Algorithm 1.

Structure Completion. For structure completion, we use the log-likelihood function defined in (10):

$$f(\mathbf{y}, \mathbf{z}) = - \left\| \begin{pmatrix} \mathbf{I}_m & 0 \\ 0 & 0 \end{pmatrix} \mathbf{V}^T \mathbf{z} - \mathbf{S}^+ \mathbf{U}^T \mathbf{y} \right\|_2^2.$$
 (15)

Model Refinement. In the model refinement task, we combine three sources of information with the following three log-likelihood functions:

$$f_{m}(\bar{\mathbf{x}}, \mathbf{z}) = - \left\| \begin{pmatrix} \mathbf{I}_{m} & 0 \\ 0 & 0 \end{pmatrix} \mathbf{V}^{T} \mathbf{z} - \mathbf{S}^{+} \mathbf{U}^{T} \bar{\mathbf{x}} \right\|_{2}^{2}$$
 (incomplete model)

$$f_{s}(\mathbf{s}, \mathbf{z}) = \log p_{\theta}(\mathbf{s} | \mathbf{R} \mathbf{z}, t = 0)$$
 (sequence)

$$f_{d}(\mathbf{y}, \mathbf{z}) = - \|\mathbf{y} - \mathcal{B}(\Gamma(\mathbf{R} \mathbf{z}, \mathbf{s}, \chi))\|_{2}^{2}, \text{ where } \chi \sim p_{\theta}(\chi | \mathbf{R} \mathbf{z}, \mathbf{s}, t = 0)$$
 (cryo-EM density)

 Γ is an operator turning an all-atom model into a density map. Given $\mathbf{X}=(\mathbf{x},\mathbf{s},\chi)=[X_1,\ldots,X_A]^T\in(\mathbb{R}^3)^A$, the Cartesian coordinates of A heavy atoms,

$$\Gamma(\mathbf{X}): x \in \mathbb{R}^3 \mapsto \sum_{i=1}^A \sum_{j=1}^5 4\pi \frac{a_{i,j}}{b_{i,j}} \exp\left(-\frac{4\pi^2}{b_{i,j}} \|X_i - x\|_2^2\right) \in \mathbb{R},\tag{17}$$

where $a_{i,j}$ and $b_{i,j}$ are tabulated form factors [24]. The norm $\|\mathbf{y} - \Gamma(\mathbf{X})\|_2^2$ is computed directly in Fourier space using Parseval's theorem, up to a time-dependent resolution r_t . Here, we assume the B-factors are unknown and we neglect their contribution in the log-likelihood function as we consider high-resolution density maps ($\leq 4 \text{ Å}$).

Pairwise Distances to Structure. We use the following log-likelihood function:

$$f(\mathbf{y}, \mathbf{z}) = -\|\mathbf{y} - \|\mathbf{D}\mathbf{R}\mathbf{z}\|_2\|_2^2. \tag{18}$$

B Optimization parameters

Structure Completion. All experiments are ran for 1,000 epochs, with a learning rate λ of 0.3 and a momentum ρ of 0.9. The time schedule is linear:

$$t = 1 - \text{epoch}/1000.$$
 (19)

Model Refinement. All experiments are ran for 4,000 epochs. The learning rates are

$$\lambda_m = 0.1, \quad \lambda_s = \begin{cases} 0 \text{ if epoch } < 3,000 \\ 1 \times 10^{-5} \text{ otherwise} \end{cases}, \quad \lambda_d = 3 \times 10^{-5} \cdot (r_t/r_0)^3, \tag{20}$$

and all the momenta are set to 0.9. r_t is set to 15 Å for the first 3,000 epochs and linearly decreases to 5 Å during the last 1,000 epochs. The side chain angles (χ) are sampled every 100 epochs. The time schedule is

$$t = 1 - \sqrt{\frac{\text{epoch}}{4,000}}.$$
 (21)

Pairwise Distances to Structure. All experiments are ran for 1,000 epochs, with a learning rate $\lambda = 200/n$, where n is the number of known pairwise distances, and a momentum ρ of 0.99. The time schedule is

$$t = 1 - \sqrt{\frac{\text{epoch}}{1,000}}.$$
 (22)

C Correlated Diffusion

We use the " R_q -confined globular polymer" correlation matrix, as defined in [29]:

$$\mathbf{R} = a \begin{bmatrix} \nu b^{0} \\ \nu b^{1} & b^{0} \\ \nu b^{2} & b^{1} & b^{0} \\ \vdots & \ddots & \ddots \\ \nu b^{N-2} & b^{1} & b^{0} \\ \nu b^{N-1} & \cdots & b^{2} & b^{1} & b^{0} \end{bmatrix},$$
(23)

where a is a free parameter, $\nu=\frac{1}{\sqrt{1-b^2}}$ and b is chosen such that the radius of gyration R_g scales with the number of residues as $R_g\sim rN^\alpha$ ($r\approx 2.0$ Å, $\alpha\approx 0.4$ [63, 27]).

D Target Structures

Information on the proteins used as target structures are given in Table 1.

Table 1: Information on target structures.												
PDB	Nb. of residues	Resolution	Release date	Imaging method	€ CASP15							
7r5b	127	1.77 Å	2023-02-08	X-ray diffraction	No							
7qum	130	1.50 Å	2023-03-01	X-ray diffraction	No							
1cfd	148	N/A	1995-12-07	NMR	No							
7pzt	160	1.84 Å	2022-11-02	X-ray diffraction	Yes							
1a2f	291	2.10 Å	1998-11-25	X-ray diffraction	No							

Table 1: Information on target structures

E Additional Results

E.1 Structure Completion

We provide additional results in Table 2. The Evidence Lower Bound (ELBO) is computed with Chroma and is a lower bound of the learned log-prior. Note that, as the subsampling factor increases (i.e., as the problem becomes less constrained), the gap between our approach (MAP estimation) and the baseline (low-temperature posterior sampling) decreases. For highly undersampled structures, the RMSD with the target structure is high but the generated structure remains plausible under the learned prior distribution.

E.2 Gradient Descent for Linear Constraints

In Figure 6, we compare different gradient-based techniques for minimizing over z the following objective function:

$$\mathcal{L}(\mathbf{z}) = \|\mathbf{M}\mathbf{x}^* - \mathbf{M}\mathbf{R}\mathbf{z}\|_2^2. \tag{24}$$

 \mathbf{x}^* is the backbone structure of the ATAD2 protein (PDB:7qum). \mathbf{M} is a masking matrix with a subsampling factor of 2. The preconditioning strategy is described in Section 4.2. Gradient descent with preconditioning and momentum leads to the fastest convergence.

E.3 Ablation Study for Model Refinement

In Figure 7, we analyze the importance of the different input measurements for atomic model refinement. Removing the partial atomic model leads to the largest drop in accuracy. The cryo-EM density map is the second most important measurement, followed by the generative prior and the sequence.

Table 2: Additional structure completion results. We compare our method to Chroma [29] with a SubstructureConditioner. We report the RMSD in \mathring{A} (best of 8) and the associated Evidence Lower Bound (ELBO) provided by Chroma as a proxy for realism.

DDD (# mag.)	Metric	Mothod	Subsampling factor						
PDB (# res.)		Method	2	4	8	16	32	64	128
	RMSD (↓)	Chroma*	0.41	1.34	3.73	9.34	15.95	16.27	_
7r5b (127)		ADP-3D	0.10	0.47	2.21	4.47	9.45	11.54	_
. 100 (127)	ELBO (†)	Chroma*	7.79	6.72	7.27	7.56	7.40	9.10	_
		ADP-3D	7.38	7.87	7.48	6.65	7.64	7.98	_
	RMSD (↓)	Chroma*	0.28	0.81	2.14	3.46	7.70	11.49	14.45
7qum (130)		ADP-3D	0.21	0.27	1.13	2.68	5.60	7.76	13.01
. 4 (100)	ELBO (†)	Chroma*	5.87	6.08	7.16	7.13	8.43	8.89	9.27
		ADP-3D	5.64	6.47	7.87	7.56	7.99	8.76	8.98
	RMSD (↓)	Chroma*	0.42	1.17	3.06	5.84	9.44	14.28	15.87
1cfd (148)		ADP-3D	0.20	0.59	1.83	4.62	12.76	12.51	15.29
	ELBO (†)	Chroma*	5.65	5.97	6.49	5.46	8.87	9.22	8.94
		ADP-3D	5.22	5.34	7.60	8.00	8.91	8.72	7.82
	RMSD (↓)	Chroma*	0.50	1.61	4.82	10.36	16.15	16.81	16.93
7pzt (160)		ADP-3D	0.23	0.67	2.64	9.39	14.26	15.47	14.07
1	ELBO (†)	Chroma*	5.99	5.55	5.39	7.47	8.52	8.74	9.04
		ADP-3D	5.79	6.44	6.92	7.79	8.29	7.81	8.64
	RMSD (\downarrow)	Chroma*	0.39	1.21	3.42	7.45	14.77	16.99	17.29
1a2f (291)		ADP-3D	0.13	0.68	1.91	5.48	12.48	17.78	19.68
()	ELBO (†)	Chroma*	5.39	5.33	6.83	7.09	8.74	9.28	9.48
		ADP-3D	5.24	6.54	7.62	7.85	8.20	8.27	9.12

E.4 Additional video

We provide one additional video showing the predicted structure throughout the diffusion process, for the three tasks explored in this paper.

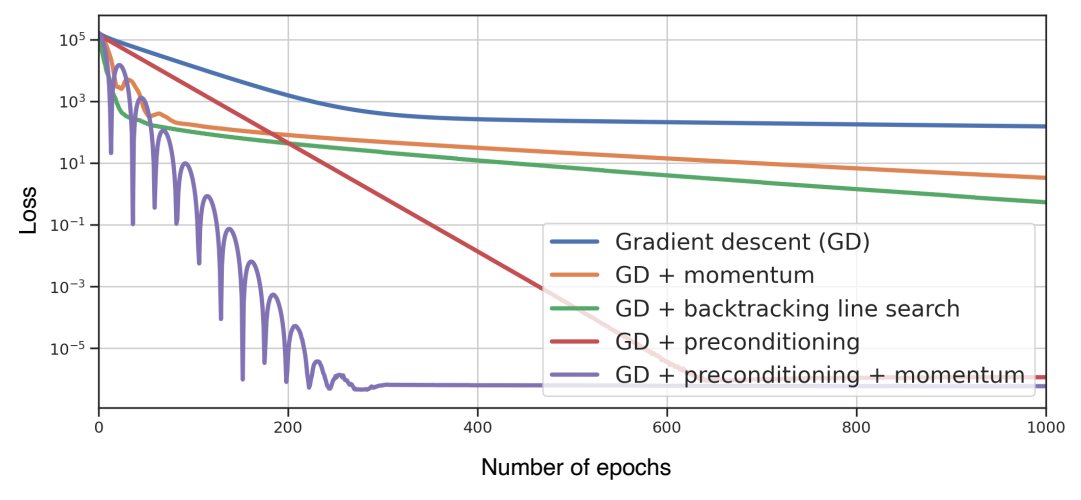


Figure 6: Gradient Descent for Linear Constraint. Convergence speed of different techniques on a linear inverse problem (structure completion with a subsampling factor of 2), without the diffusion prior. Using preconditioning with momentum leads to the fastest convergence. The "loss" corresponds to the negative log-likelihood.

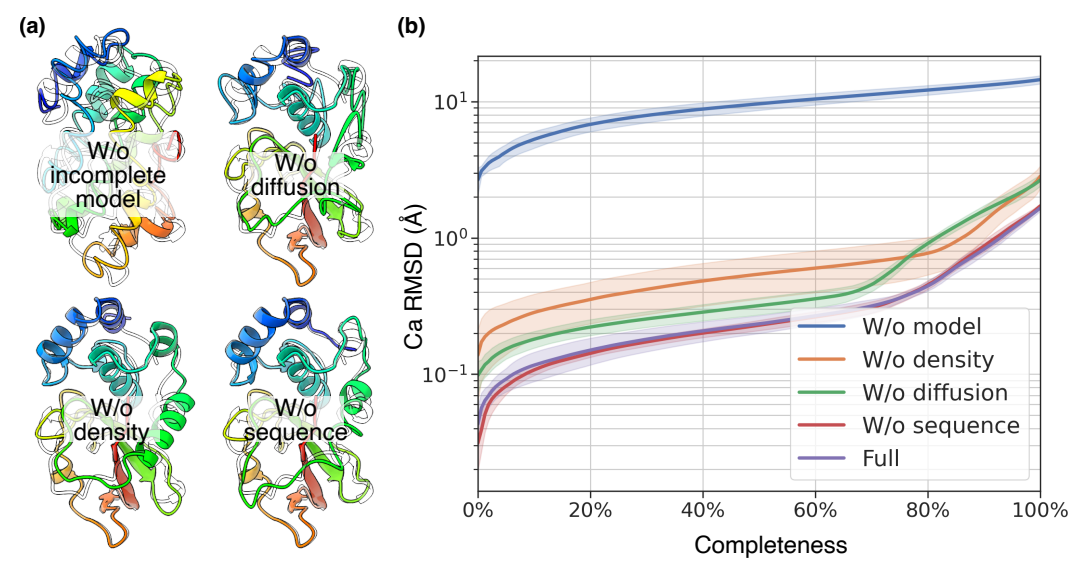


Figure 7: Ablation Study. For atomic model refinement, we combine three sources of conditioning information (incomplete model, density map and sequence) with the data-driven prior of the diffusion model. Here we highlight the importance of each conditioning information, and that of the generative prior. (a) Qualitative reconstructions with the target structure in transparency. (b) RMSD of alpha carbons vs. completeness. We use the same structure as in Fig. 4 (PDB:7pzt), and a cryo-EM map at 2.0 Å resolution.